BMC Veterinary Research

RESEARCH

Open Access

Untargeted metabolomics reveals alternations in metabolism of bovine mammary epithelial cells upon IFN-γ treatment

Fengyang Li[1†], Xiuhong Hu[2,3†], Zengshuai Wu[1†], Qiulei Yang[1], Qila Sa[1], Wenbo Ren[2], Tingting Wang[2], Zhengchao Ji[2], Na Li[1*], Jing Huang[2*] and Liancheng Lei[1*]

Abstract

Background IFN-γ is a pleiotropic cytokine that has been shown to affect multiple cellular functions of bovine mammary epithelial cells (BMECs) including impaired milk fat synthesis and induction of malignant transformation via depletion of arginine, one of host conditionally essential amino acids. But the molecular mechanisms of these IFN-γ induced phenotypes are still unknown.

Methods BMECs were treated with IFN-γ for 6 h, 12 h, and 24 h. The metabolomic profiling in BMECs upon IFN-γ induction were assessed using untargeted ultra-performance liquid chromatography-mass spectrometry (UPLC-MS) metabolomic analysis. Key differentially expressed metabolites (DEMs) were quantified by targeted metabolomics.

Results IFN-γ induction resulted in significant differences in the contents of metabolites. Untargeted analysis identified 221 significantly DEMs, most of which are lipids and lipid-like molecules, organic acids and derivatives, organ heterocyclic compounds and benzenoids. According to Kyoto Encyclopedia of Genes and Genomes (KEGG) pathway analysis, DEMs were enriched in fructose and mannose metabolism, phosphotransferase system (PTS), β-alanine metabolism, arginine and proline metabolism, methane metabolism, phenylalanine metabolism, and glycolysis/gluconeogenesis. Quantification of selected key DEMs by targeted metabolomics showed significantly decreased levels of D-(-)-mannitol, argininosuccinate, and phenylacetylglycine (PAG), while increased levels in S-hydroxymethylglutathione (S-HMG) and 2,3-bisphospho-D-glyceric acid (2,3-BPG).

Conclusions These results provide insights into the metabolic alterations in BMECs upon IFN-γ induction and indicate potential theoretical basis for clarifying IFN-γ-induced diseases in mammary gland.

Keywords IFN-γ, Arginine depletion, Malignant transformation, Bovine mammary epithelial cells, Metabolomics

†Fengyang Li, Xiuhong Hu and Zengshuai Wu contributed equally to this work.

*Correspondence:
Na Li
vetlina2013@126.com
Jing Huang
huangj@jlu.edu.cn
Liancheng Lei
leiliancheng@163.com
[1] State Key Laboratory for Zoonotic Diseases, College of Veterinary Medicine, Jilin University, 1977 Xinzhu Road, Changchun 130062, China
[2] Department of First Hospital, Jilin University, 1 Xinmin Street, Changchun 130021, China
[3] Shannan Hospital, Shannan 856099, China

Introduction

Arginine is a conditional essential amino acid depending on the growth stage and body condition. For young mammals, arginine is one of the essential amino acids because of its low content in the breast milk and insufficient arginine synthesis [1]. On the other hand, endogenous synthesis of arginine can meet the demand of body's basal metabolism which makes it is a non-essential amino acid for adults. As the most abundant nitrogen carrier in proteins, arginine is the substrate for the synthesis of multiple substances including proteins, urea, ornithine, nitric oxide (NO), creatine, polyamines, nucleotides, proline, and agmatine [2, 3]. Thus, arginine plays vital roles in many biologic processes, including nutrients metabolism, cell growth and proliferation, release of hormone, and immune responses [4, 5].

In pathological conditions, cells under various stress factors are accompanied by abnormal arginine metabolism, resulting in significant reduction of intracellular arginine or arginine depletion. Many studies have found that arginine depletion is closely associated with the development of many diseases, such as cancer and infection [6, 7]. Arginine is required for tumor cell growth and actually, many tumor types including human breast cancer are arginine auxotrophic [8, 9], which makes arginine depletion an efficient therapeutic strategy for auxotrophic cancer treatment. However, a study by Cao et al. demonstrates that arginine supplementation inhibits the growth of breast cancer cells by enhancing innate and adaptive immune responses that are mediated by myeloid-derived suppressor cells in vivo [10]. Moreover, arginine also contributes to host immune defense in response to pathogenic infections. Arginine supplementation reduces the inflammatory response and susceptibility to *Staphylococcus aureus* (*S. aureus*) of bovine mammary epithelial cells (BMECs) and protects host from mastitis in vivo [11].

The influencing factors and mechanism of arginine depletion are poorly studied. Interestingly, arginine metabolism is influenced by IFN-γ, a pleiotropic inflammatory cytokine which usually involves in inflammation and autoimmune diseases [12, 13]. It's found that the level of IFN-γ was closely associated with arginine depletion, suggesting IFN-γ possibly disorders arginine metabolism and leads to occurrence of diseases. Mice fed gluten-containing standard diet shows elevated IFN-γ level which may contribute to the higher type 1 diabetes incidence [14]. Arginine depletion reduces the expression of natural killer (NK) cell receptors and intracellular production of IFN-γ, which hinder NK cell functions [15]. Studies from our group demonstrate that IFN-γ induces arginine depletion that increase susceptibility to *S. aureus* and mastitis occurrence, impairs milk fat and protein synthesis, and malignant transformation of bovine mammary epithelial cells (BMECs) [11, 16, 17]. These results suggest that the regulation of arginine by IFN-γ might be therapeutic targets of some diseases. However, the exact mechanism for IFN-γ-induced arginine depletion of cells including BMECs is still unknown.

Metabolomics is a widely used tool to analyze the changes of various small molecule metabolites in systematic and molecular biology [18, 19]. Using high-throughput in silico analysis of metabolomics data, characteristic differentially expressed metabolites (DEMs) which reflect the functional status of living organisms can be identified without discrimination [20]. In this study, an untargeted and targeted metabolomics approach involving ultra-performance liquid chromatography-mass spectrometry (UPLC-MS) was applied to explore the mechanism underlying how IFN-γ induces arginine depletion of BMECs. All DEMs upon IFN-γ induction were identified and enriched by Kyoto Encyclopedia of Genes and Genomes (KEGG) pathway analysis [21–23]. Our study not only contributes to better understanding the arginine metabolism of BMECs, but also provides a molecular basis for the occurrence and prevention of diseases associated with IFN-γ-induced abnormal arginine metabolism.

Materials and methods

Chemicals and reagents

Bovine IFN-γ was purchased from the Kingfisher Biotech (S. Paul, MN, USA). LC–MS grade methanol and formic acid (98%) were bought from Sigma-Aldrich (St. Louis, MO, USA); acetonitrile was bought from Thermo (Shanghai, China). Ultrapure water was obtained with a Milli-Q system (Millipore Co., MA, USA). All chemicals and solvents used were of analytical or HPLC grade.

Sample preparation for untargeted metabolic analysis

The BMECs cell line, MAC-T [24] (provided by Prof. Guoqiang Zhu, Yangzhou University, Yangzhou, China), was used in this study. All the cells were grown in Dulbecco's modified Eagle's medium/nutrient mixture F-12 (DMEM/F12) with 10% fetal bovine serum (FBS, CLARK, China), with 100 U/mL penicillin, 100 mg/mL streptomycin and incubated at 37 °C in a humidified atmosphere with 5% CO_2. When entered the logarithmic growth phase, the cells were digested using 0.25% trypsin. For untargeted metabolomics detection, cells were treated with IFN-γ for different time periods 6 h, 12 h, and 24 h. After trypsin digestion and centrifugation at 1000 rpm for 10 min, the cell pellets were harvested and re-suspended in 1 mL pre-cooled PBS, followed by addition of 5 mL pre-cooled quenching reagent (8.6 g/L NH_4HCO_3 pH = 7.4, 60% ethanol), mixed evenly and

centrifuged at 6000 g for 15 min at 4 °C. The cell pellets were re-suspended in 2 mL ultra-pure water and were sonicated in an ice bath for 10 min (5 s sonication with 5 s interval). The protein precipitation reagent (methanol: acetonitrile: water = 2: 2: 1, v/v/v) was added, mixed uniformly and centrifuged at 13,000 g, 4 °C for 15 min. The supernatant was collected for further analysis.

Quality control (QC) sample preparation for untargeted metabolic analysis

Quality control samples (QC) were prepared by taking out same amount (50 μL) of volume from each group of samples. A total of 200 μL of each sample were dried and concentrated on a nitrogen blower at 37 °C, and dissolved in 50 μL of protein precipitation reagent in ampoules for further test.

Sample detection by UPLC-MS for untargeted metabolic analysis

Liquid chromatography was performed with ExionL CAD UPLC equipped with a TripleTOF 5600 MS system. The samples were separated by an ACQUITY UPLC HSS T3 column (2.1 × 100 mm, 1.8 μm) at 35 °C, the injection volume was 5.0 μL. Mobile phase A: 0.1% formic acid; mobile phase B: 95% acetonitrile. Samples elution was performed at a flow rate of 0.35 mL/min. Gradient elution procedure was as follows: 0 - 0.5 min, 2% B; 0.5 -1.5 min, 2% - 20% B; 1.5 - 4.0 min, 20% - 65% B; 4.0 - 11.0 min, 65% - 95% B; 11.0 min - 15.0 min, 95% B; 15.0 min - 15.1 min, 95% - 2% B; 15.1 min - 20.0 min, 2% B. Samples were detected by electrospray ion source in both positive and negative ion modes. Samples were scanned with following parameters: DP = 100 V, CE = 35 eV, 100 - 1000 Da, curtain gas (CUR) = 30 psi, atomizing gas (GS1) = 55 psi, heating gas (GS2) = 55 psi, ion spray voltage (ISVF) = 5500 V, ion source temperature = 550 °C.

Sample preparation for targeted metabolic analysis

Sample preparation for targeted metabolomics was performed as previously reported [25]. Reagents and materials for targeted metabolomics analysis are the same as those for nontargeted metabolomics. Briefly, the metabolite standards and the internal standards were dissolved with 90% acetonitrile to a final concentration of 5 mg/mL and 1 mg/mL, respectively. 50 μL samples were mixed with 50 μL internal standard working solution, 50 μL ethyl water (acetonitrile: water = 1:1, v/v), and 350 μL acetonitrile containing 1% formic acid. The mixture was vortex-mixed and centrifuged for 10 min at 4 °C, 12,000 rpm. The supernatant was collected for further analysis by UPLC-MS.

Sample detection by UPLC-MS for targeted metabolic analysis

Liquid chromatography was performed with ExionL CAD UPLC equipped with a TripleTOF 5600 MS system. The samples were separated by a ZORBAX Eclipse XDB-C8 column (4.6 × 150 mm, 5 μm) at 30 °C, the injection volume was 15.0 μL. Mobile phase A: 0.1% formic acid; mobile phase B: 95% acetonitrile. Samples elution was performed at a flow rate of 0.2 mL/min. Gradient elution procedure is as follows: 0 - 2.5 min, 2% B; 2.5 - 4.0 min, 2% - 50% B; 4.0 - 6.0 min, 50% B; 6.0 - 6.1 min, 50% - 5% B; 6.1 min - 9.9 min, 5% B; 9.9 min - 10.0 min, 2% B. Samples were detected by electrospray ion source in positive ion mode. Samples were scanned with following parameters: DP = 60 V, CE = 10 eV, 50 - 250 Da, curtain gas (CUR) = 30 psi, atomizing gas (GS1) = 50 psi, heating gas (GS2) = 50 psi, ion spray voltage (ISVF) = 5500 V, ion source temperature = 500 °C.

Data processing and analysis

The MS raw data were analyzed by Progenesis QI 2.3 software (Nonlinear Dynamics, WatersCorp, Durham, USA). Data of different samples were aligned according to the retention time deviation of 0.2 min and the mass deviation of 5 ppm, and analyzed according to the coefficient of variation (CV) value of 30%, signal-to-noise ratio of 3, minimum signal strength of 100,000. The significant differences of metabolites were verified by variable weight value (VIP) > 1.0, fold change (FC) > 2.0 or FC < 0.5 and $p < 0.05$. Experimental data were statistically analyzed by GraphPad (version 9.0). Data were presented as the mean ± standard deviation (SD) from three independent replicates. The differences between the mean values of normally distributed data were assessed by one-way ANOVA (Dunnett's test). $p < 0.05$ was considered as statistically significant, which was indicated by "*". $p < 0.01$ indicated that the difference was extremely significant, which was indicated by "**".

Results

Detection of metabolites

To evaluate the metabolic alternations induced by IFN-γ in BMECs, we detected the metabolites in samples of IFN-γ treatment group and control group at different time (6 h, 12 h and 24 h) by untargeted metabolomics analysis in both negative and positive ion modes. Validation of the analytical method was achieved using quality control (QC) samples. The correlation heat map showed that the correlation coefficient among QC

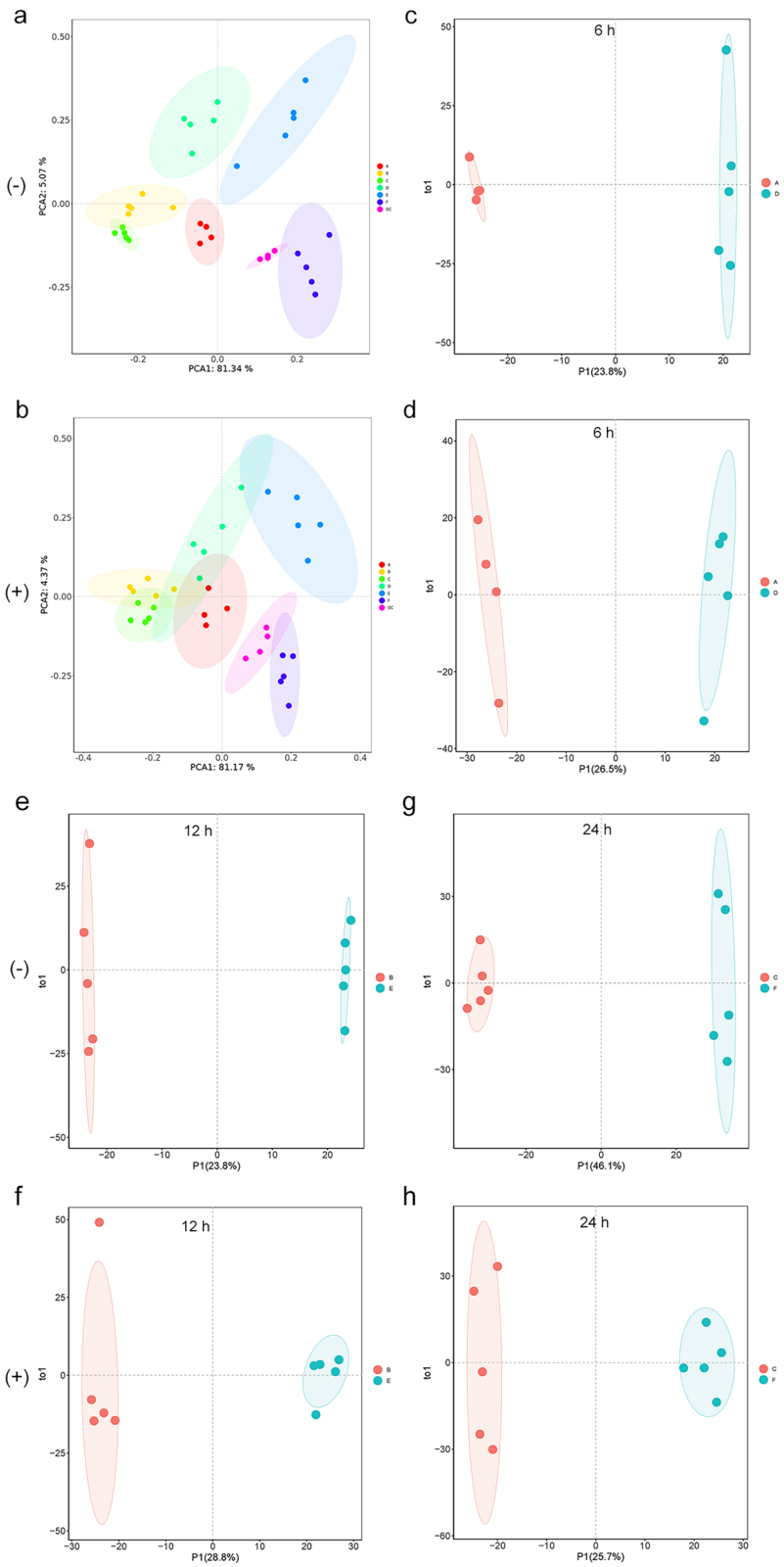

Fig. 1 Multivariate statistical analysis of samples in positive and negative ion modes. Principal components analysis (PCA) in negative (**a**) and positive (**b**) ion modes; orthogonal partial least-squares discriminant analysis (OPLS-DA) score chart in negative (**c, e, g**) and positive (**d, f, g**) ion modes. Figure c, e, and g: control cells incubated for 6 h, 12 h, and 24 h, respectively; d, f, and h: cells stimulated with IFN-γ for 6 h, 12 h, and 24 h, respectively. (-), negative ion mode. (+), positive ion mode. QC, quality control

samples in both ionization modes was almost 1.0 (from 0.983 to 1.000) (Fig. S1), which indicates that the detection method has good stability and reproducibility of QC samples. According to the qualitative metabolite results, a total of 4,762 substance peaks (including 2,543 negative ion peaks and 2,219 positive ion peaks) in samples were detected. Furthermore, 2,253 annotated metabolites, including 976 negative ion mode metabolites and 1,277 positive ion mode metabolites, were identified.

Multivariate data analysis

Next, unsupervised principal component analysis (PCA) and orthogonal partial least squares discriminant analysis (OPLS-DA) was utilized to discriminate the overall distribution among samples. In the negative ion mode, the first and second principal components (PCA1 and PCA2) accounted for 81.34% and 5.07% of the total variance, respectively. While in the positive ion mode, the first and second principal components (PCA1 and PCA2) accounted for 81.17% and 4.37% of the total variance, respectively. The PCA showed clear differences among the groups in both ion modes, especially before and after IFN-γ induction (Fig. 1a and b). As time grows, the differences among control groups and IFN-γ induction groups, and the differences between control group and IFN-γ induction group gradually expanded, indicating there may have been significant differences in the expression of metabolites upon IFN-γ induction in BMECs. Similarly, the OPLS-DA model also displayed clear segmentation between the two groups in both ion modes (Fig. 1c-h). The permutation test of the OPLS-DA model showed that the interpretation rate ($R^2Y(CUM)$) for the sample was close to 1 and the predictive ability ($Q^2(CUM)$) was greater than 0.47 (Fig. S2), indicating that the model was reliable and can better explain and predict the differences in samples among the groups.

Identification of differentially expressed metabolites

To further identify the differentially expressed metabolites (DEMs) in the samples, we screened the metabolites using variable importance projection (VIP) > 1, fold change (FC) > 2.0 or FC < 0.5 and p-value < 0.05 in the OPLS-DA model. After data acquisition and analyzation, a total of 108 and 113 DEMs were screened out in negative and positive ion modes, respectively (Table S1). Compared to control, there were 11 significantly DEMs (1 upregulated, 10 downregulated) upon IFN-γ treatment for 6 h (Table S2; Fig. 2a); 14 significantly DEMs (3 upregulated, 11 downregulated) upon IFN-γ treatment for 12 h (Table S3; Fig. 2b); and 25 significantly DEMs (14 upregulated, 11 downregulated) upon IFN-γ treatment for 24 h (Table S4; Fig. 2c). Compared to IFN-γ treatment for 6 h group, there were 27 significantly DEMs (11 upregulated, 16 downregulated) upon IFN-γ treatment for 12 h (Table S5; Fig. 2d); 86 significantly DEMs (37 upregulated, 49 downregulated) upon IFN-γ treatment for 24 h (Table S6; Fig. 2e). Compared to IFN-γ treatment for 12 h group, there were 58 significantly DEMs (13 upregulated, 45 downregulated) upon IFN-γ treatment for 24 h (Table S7; Fig. 2f). The volcano plots between each comparison group displayed the DEMs that contributed to the sample separation (Fig. 2a-f). Subsequently, we applied hierarchical clustering analysis and found that DEMs were distinguishable in the heat map (Fig. 3a and b). According to the Human Metabolome Database (HMDB), the majority of different metabolites were lipids and lipid-like molecules; organic acids and derivatives; organ heterocyclic compounds; benzenoids; phenylpropanoids and polyketides; and organic oxygen compounds (Fig. 4a). Furthermore, the majority of identified lipids belong to fatty acid conjugates, fatty amides, glycerophosphocholines, glycerophosphoethanolamines, and fatty esters according to the LIPID MAPS Structure Database (LMSD) classification (Fig. 4b).

KEGG pathway enrichment analysis

Subsequently, we analyzed the different metabolic pathways enrichment using the KEGG database [21–23]. The results showed that the DEMs were enriched in 141 and 115 KEGG metabolic pathways in negative and positive ion modes, respectively. The different metabolic classifications upon IFN-γ treatment are mainly enriched in category metabolism including lipid metabolism, amino acid metabolism, chemical structure transformation maps, nucleotide metabolism, and metabolism of cofactors and vitamins; organismal systems including digestive system; human diseases including cancer; environmental information processing including membrane transport (Fig. 5a). We then analyzed the top pathways with significant KEGG enrichment in both ion modes. Interestingly, many of the DEMs are not annotated in KEGG database. Specifically, the pathways of DEMs in IFN-γ treatment for 12 h group were mainly concentrated in fructose and mannose metabolism (00051,

(See figure on next page.)

Fig. 2 Volcano plots for the differentially expressed metabolites (DEMs) in negative and positive ion modes. (**a**) control (6 h) versus IFN-γ stimulation (6 h); (**b**) control (12 h) versus IFN-γ stimulation (12 h); (**c**) control (24 h) versus IFN-γ stimulation (24 h); (**d**) IFN-γ stimulation (12 h) versus IFN-γ stimulation (6 h); (**e**) IFN-γ stimulation (24 h) versus IFN-γ stimulation (12 h); (**f**) IFN-γ stimulation (24 h) versus IFN-γ stimulation (6 h). Downregulated or upregulated genes were divided by |log2Ratio| ≥ 1 with false discovery rate (FDR) ≤ 0.01. Red dots for upregulated genes and dark blue dots for downregulated genes. vs, versus. (-), negative ion mode. (+), positive ion mode

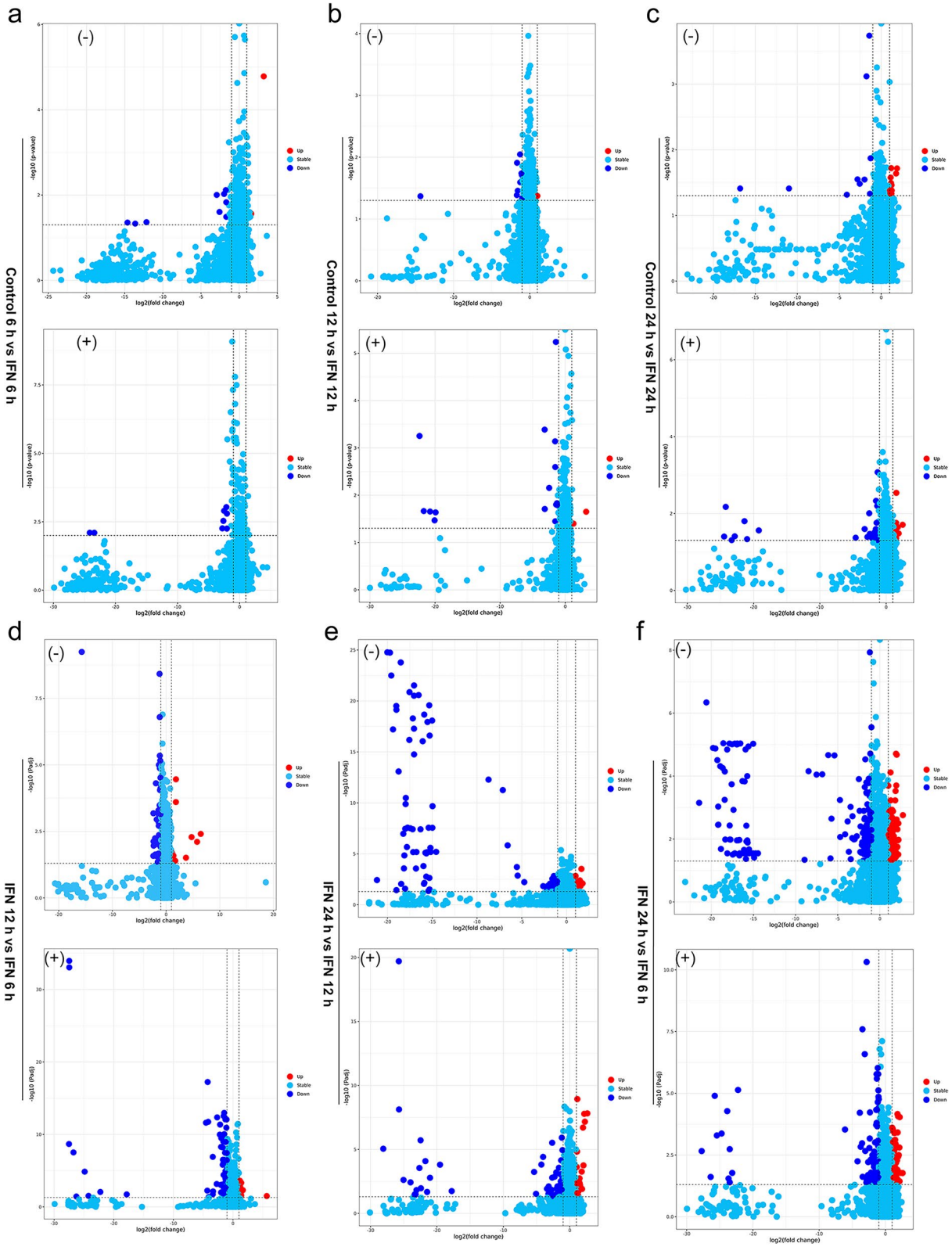

Fig. 2 (See legend on previous page.)

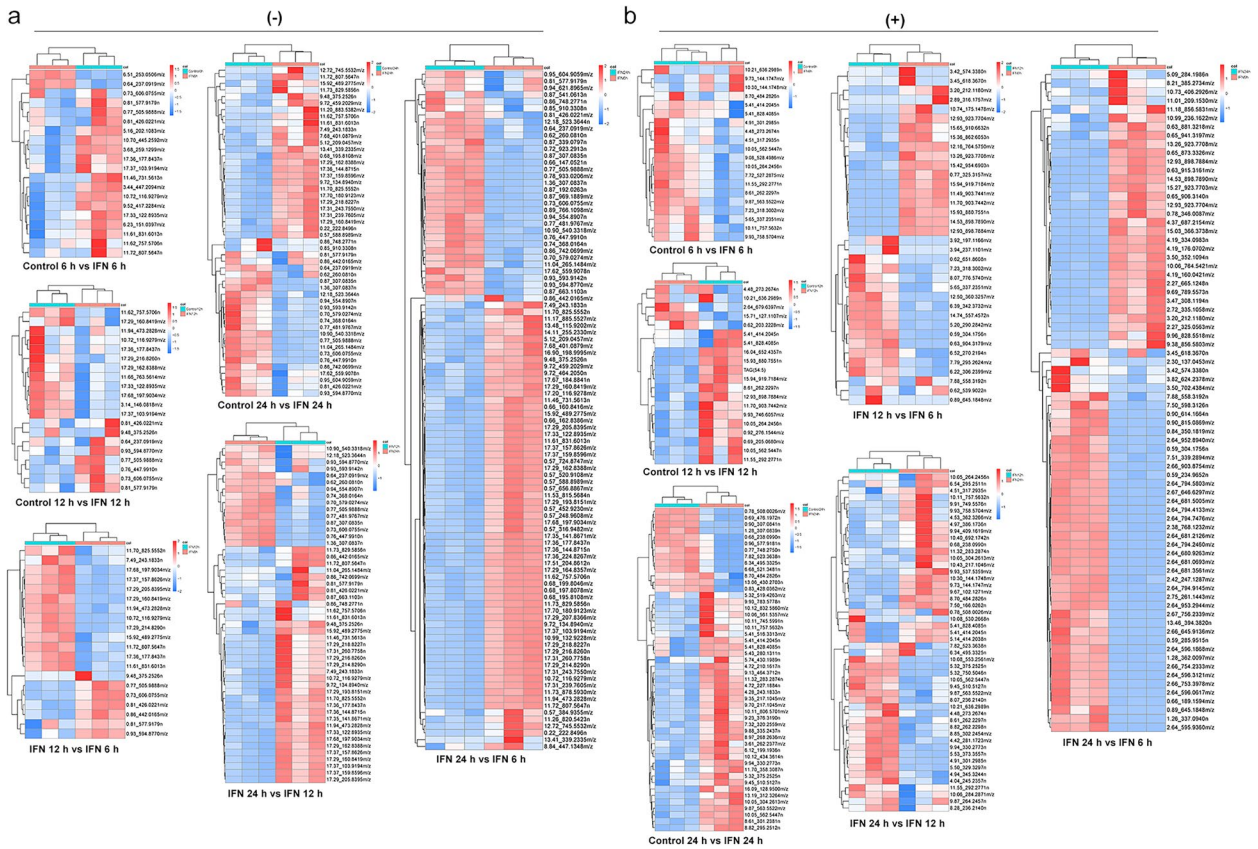

Fig. 3 Heatmap of the differentially expressed metabolites (DEMs) in negative (**a**) and positive (**b**) ion modes. DEGs were screened out according to |log2Ratio|≥ 1 with false discovery rate (FDR) ≤ 0.01. Red rectangles indicate upregulated metabolites and blue rectangles indicate downregulated metabolites. (-), negative ion mode. (+), positive ion mode

Fig. S3), phosphotransferase system (PTS) (02060, Fig. S4), β-alanine metabolism (00410, Fig. S5), arginine and proline metabolism (00330, Fig. S6), compared to control group; while that in IFN-γ treatment for 24 h group were only methane metabolism (00680, Fig. S7) (Fig. 5b). The pathways of the DEMs in IFN-γ treatment 24 h and 12 h groups were mainly concentrated in phenylalanine metabolism (00360, Fig. S8), while those of the DEMs in IFN-γ treatment 24 h and 6 h groups were mainly concentrated in glycolysis/gluconeogenesis (00010, Fig. S9) (Fig. 5b). Overall, these results demonstrated that IFN-γ treatment led to significant metabolic changes, especially lipid and amino acid metabolism in BMECs.

Analysis of the DEMs in enriched pathways

To further analyze the DEMs enriched by KEGG classification, the contents of DEMs in significant altered pathways of each group were evaluated by enriched analysis and targeted metabolomics. All the significantly altered pathways comprised only one metabolite each (Fig. 6). Specifically, the content of D-(-)-Mannitol, in both the fructose and mannose metabolism (00051, Fig. S3) and phosphotransferase system (PTS) (02060, Fig. S4) pathways, was significantly decreased upon IFN-γ treatment for 24 h compared with control in MAC-T cells (Fig. 6A).

On the other hand, the content of spermine, in both the β-alanine metabolism (00410, Fig. S5) and arginine and proline metabolism (00330, Fig. S6) pathways, was significantly increased upon IFN-γ treatment for 12 h compared with control in MAC-T cells (Fig. 6A, Fig. S7). Previously we have shown that IFN-γ treatment did not affect ornithine level, but led to reduced intracellular levels of arginine and citrulline (Fig. S7), two of which are the key metabolites for arginine metabolism [25]. As a vital intermediate product for arginine synthesis, we further detected the intracellular level of argininosuccinate in this study. We found that the intracellular level of argininosuccinate was significantly reduced upon IFN-γ treatment (Fig. 6B), suggesting IFN-γ interferes with arginine synthesis by downregulation of argininosuccinate production in MAC-T cells.

Similarly, the content of S-hydroxymethylglutathione (S-HMG) and 2,3-bisphospho-D-glyceric acid (2,3-BPG), in methane metabolism (00680, Fig. S8) and glycolysis/

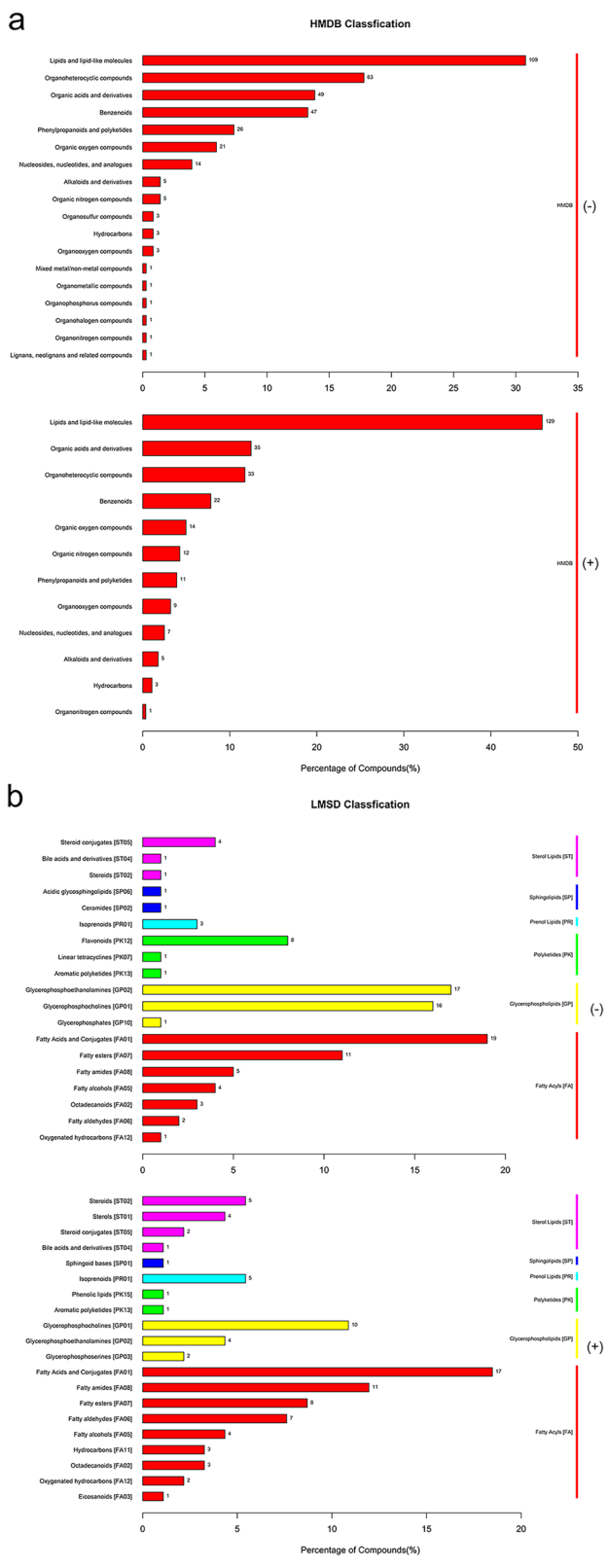

Fig. 4 HMDB (**a**) and LMSD (**b**) classifications of the different metabolites of BMECs upon IFN-γ treatment. The Y-axis indicates the HMDB/LMSD terms. The number and degree of enrichment of genes in a category is displayed in the X-axis. The *p*-value < 0.05 is defined significant. (-), negative ion mode. (+), positive ion mode. Color code: cyan, control group; red, IFN-γ treatment group

gluconeogenesis (00010, Fig. S10) pathway, respectively, was also significantly increased upon IFN-γ treatment for 24 h (Fig. 6C and D). Lastly, the content of phenylacetylglycine (PAG) in phenylalanine metabolism (00360, Fig. S9) pathway was significantly decreased upon IFN-γ treatment for 24 h compared with IFN-γ treatment for 12 h (Fig. 6E).

Discussion

In this study, untargeted and targeted metabolomics were performed using UPLC-TOF/MS to explore the mechanism for IFN-γ induced arginine depletion in BMECs. Results showed that IFN-γ induction resulted in significant differences in the contents of metabolites. KEGG pathway analysis demonstrated that most of the altered pathways were those associated with fructose and mannose metabolism, phosphotransferase system (PTS), β-alanine metabolism, arginine and proline metabolism, methane metabolism, phenylalanine metabolism, and glycolysis/gluconeogenesis.

Fructose and mannose metabolism are one of the most altered pathways in BMECs upon IFN-γ induction. We found that the content of D-(-)-Mannitol, a metabolite involves in both fructose and mannose metabolism and PTS, was significantly decreased (Fig. 6A; Fig. S3). Mannitol is widespread in both eukaryotic and prokaryotic life as a sugar or sugar alcohol. In clinical settings, mannitol has been utilized as a highly effective dehydrating agent and osmotic diuretic that contributes to minimize the risk of acute renal failure in patients after renal transplantation [26]. It facilitates excretion of water and toxic materials of tubular epithelial cells. Mannitol is also indicated as add-on maintenance therapy for improving pulmonary function in cystic fibrosis patients [27]. It is hypothesized that mannitol produces an osmotic gradient across the airway epithelium that draws fluid into the extracellular space and alters the properties of the airway surface mucus layer, which allows easier mucociliary clearance [27]. Previous results from our group demonstrated that IFN-γ induced malignant transformation of BMECs [16, 28], a precancerous phenotype with drastic cell morphology and function alternations. We assume that the downregulation of mannitol induced by IFN-γ might alters osmosis of BMECs, which leads to accumulation of toxic materials that interfere with cell normal functionality.

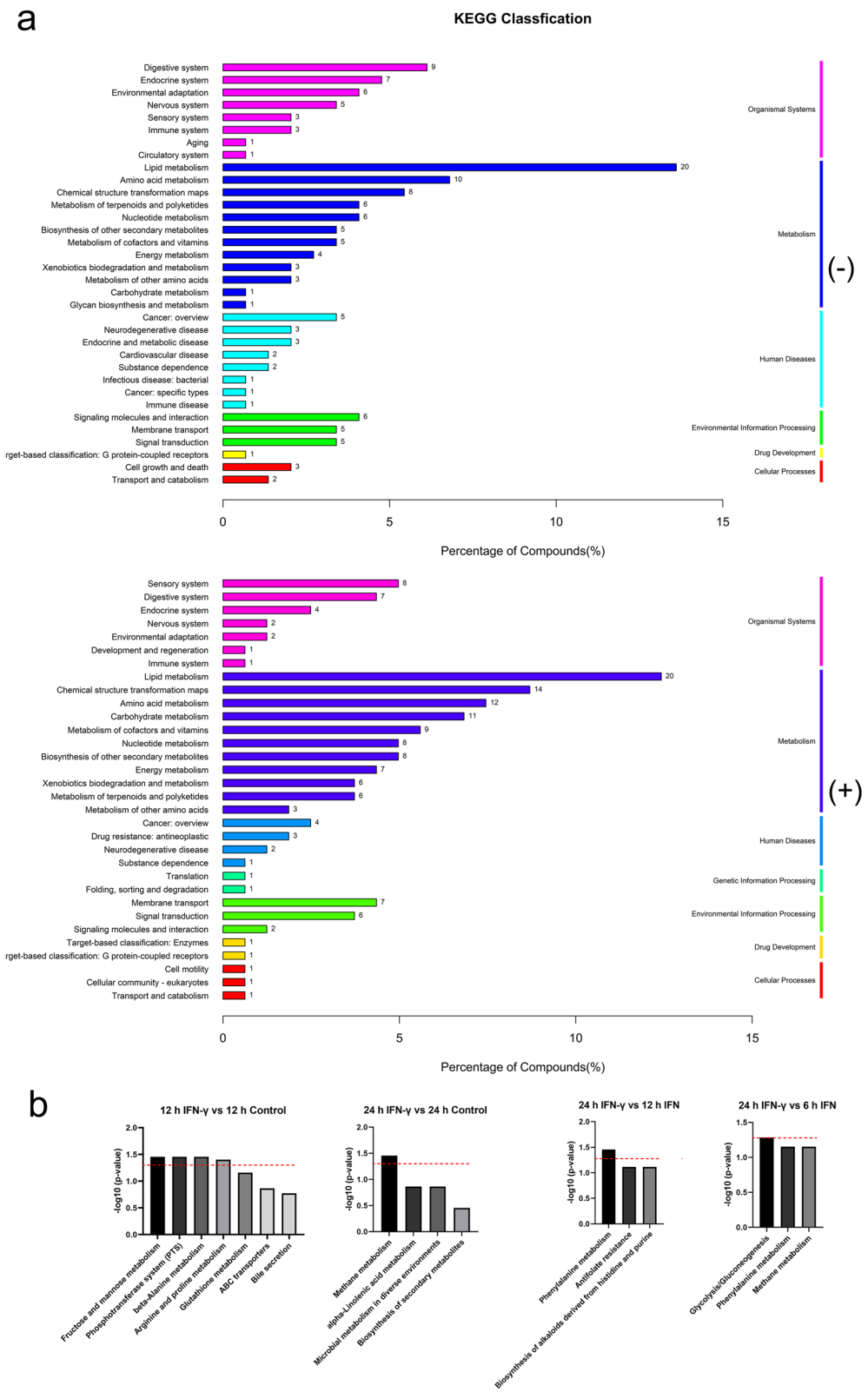

Fig. 5 KEGG pathway enrichment analysis [21–23] based on differentially expressed metabolites (DEMs) upon IFN-γ treatment. (**a**) The KEGG classifications of the DEMs. The Y-axis indicates the KEGG terms. The number and degree of enrichment of pathways in a category is displayed in the X-axis. (**b**) The main enriched KEGG pathways of the DEMs. Red dotted lines indicate *p*-value = 0.05, which is defined as significant. (-), negative ion mode. (+), positive ion mode

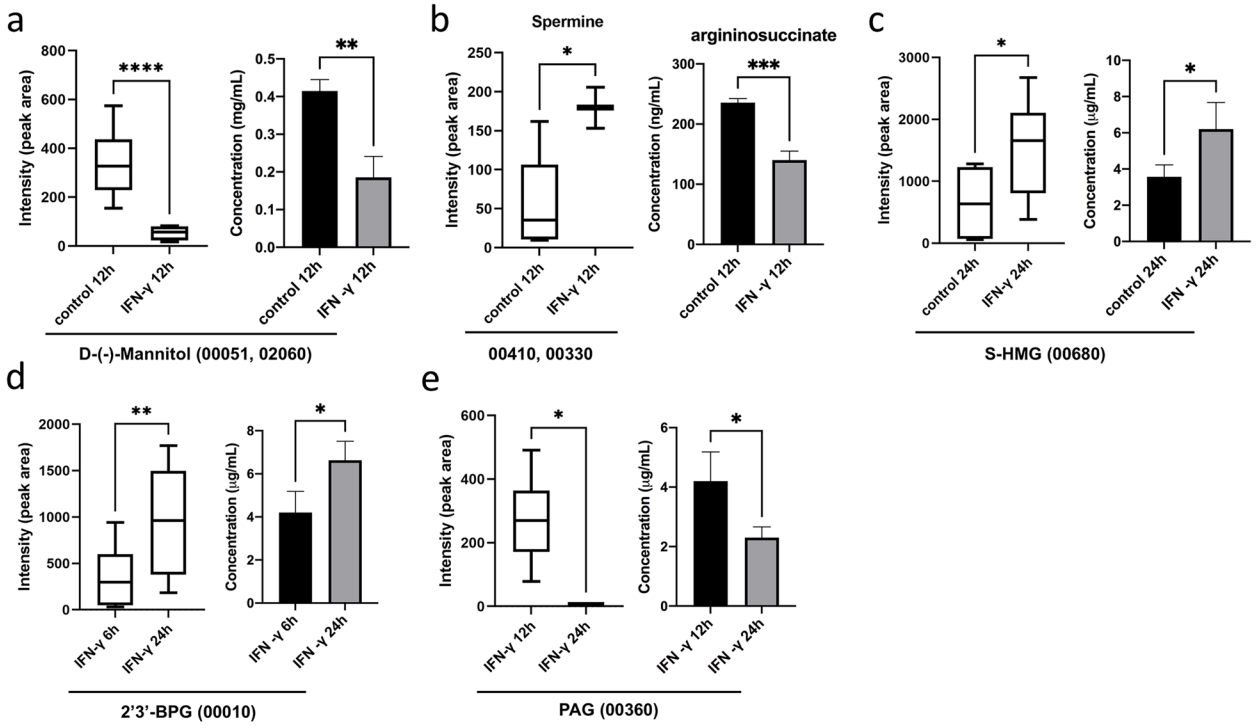

Fig. 6 Quantification of the DEMs enriched in seven important pathways by targeted metabolomics. 00051, mannose metabolism pathway; 02060, phosphotransferase system (PTS) pathway; 00410, β-alanine metabolism pathway; 00330, arginine and proline metabolism pathway; 00680, methane metabolism pathway; 00010, glycolysis/gluconeogenesis pathway; 00360, phenylalanine metabolism pathway. Differences between mean values were assessed by two-tailed Student's *t*-test. *$p < 0.05$; **$p < 0.01$; ***$p < 0.001$

Spermine is one of the metabolites involve in both the β-alanine metabolism and arginine and proline metabolism pathways (Fig. 6B; Fig. S5, S6). Spermine belongs to polyamines and it is synthesized from arginine and s-adenosylmethionine [29]. It is involved in diverse functions including cell growth and differentiation in terms of DNA synthesis and stability, regulation of transcription, ion channel regulation, and protein phosphorylation [29, 30]. Notably, spermine enhances cell growth and thus the biosynthesis spermine is upregulated in cancer cells [31]. In BMECs, IFN-γ accelerates cell growth and induces malignant transformation through arginine depletion [16, 28]. It's been shown that IFN-γ could disturb arginine metabolism by affecting the expression of key time-limiting enzymes ASS1 [25, 32]. In this study, the content of spermine was downregulated, which further confirms these results and suggest that the IFN-γ-induced malignant transformation of BMECs might possibly be associated with increased spermine levels in cells.

S-hydroxymethylglutathione (S-HMG) is the spontaneous adduct of formaldehyde and glutathione. It is oxidized by S-nitrosoglutathione reductase (GSNOR) to S-formylglutathione (FGSH) in cells [33]. It's been shown that GSNOR plays an important regulatory role in smooth muscle relaxation, immune function, inflammation, neuronal development, and cancer progression [33]. In addition, GSNOR also modulates the availability of intracellular reactive nitric oxide, a molecule which functions in inflammation and cancer immunity [34]. Of note, S-HMG plays a vital role in the detoxication of formaldehyde [35]. In this study, the level of S-HMG was significantly increased upon IFN-γ induction (Fig. 6C), indicating a possible accumulation of formaldehyde in BMECs upon IFN-γ induction that might be associated with the malignant transformation of BMECs. However, whether S-HMG affects arginine metabolism or vice versa stills need to be further demonstrated.

2,3-bisphospho-D-glyceric acid (ENO1) is one of the metabolites in glycolysis/gluconeogenesis pathway (Fig. S10). It is a glycolytic enzyme that catalyzes the conversion of 2-phosphoglyceric acid to phosphoenolpyruvic acid during glycolysis [36]. Glycolysis/gluconeogenesis plays vital roles in tumorigenesis where ENO1 involves in. It has been shown that ENO1 expression was enhanced in many tumor cells [37]. ENO1 contributes to tumorigenesis by promotion of tumor proliferation, inhibition of cancer cell apoptosis, invasion and metastasis of tumor cells [36]. Interestingly, the content of ENO1

was also upregulated upon IFN-γ induction in BMECs (Fig. 6D), indicating that ENO1 might also involves in IFN-γ-induced malignant transformation of BMECs.

Lastly, the content of phenylacetylglycine in phenylalanine metabolism was significantly downregulated upon IFN-γ induction in BMECs (Fig. 6E; Fig. S9). Phenylacetylglycine is a terminal product of phenylalanine metabolism and accepted as a biomarker for phospholipidosis [38], diabetes [39], and prostate cancer [40]. However, there is limited information about the correlation between phenylacetylglycine and arginine metabolism or tumorigenesis. Thus, phenylacetylglycine might involves in IFN-γ induced arginine depletion and malignant transformation of BMECs indirectly.

In conclusion, our study reveals potential metabolites and signaling pathways in BMECs upon IFN-γ induction. IFN-γ induces arginine depletion and malignant transformation of BMECs possibly through modulation of arginine metabolism, cell osmosis, and metabolites associated with tumorigenesis, including S-HMG and ENO1. These results provide potential theoretical basis for clarifying mechanism of diseases due to abnormal IFN-γ level.

Abbreviations

BMECs	Bovine mammary epithelial cells
UPLC-MS	Ultra-performance liquid chromatography-mass spectrometry
DEMs	Differentially expressed metabolites
KEGG	Kyoto Encyclopedia of Genes and Genomes
PTS	Phosphotransferase system
NO	Nitric oxide
QC	Quality control
PCA	Principal component analysis
OPLS-DA	Orthogonal partial least squares discriminant analysis
HMDB	Human Metabolome Database
LMSD	LIPID MAPS Structure Database
S-HMG	S-hydroxymethylglutathione
2,3-BPG	2,3-Bisphospho-D-glyceric acid

Supplementary Information

The online version contains supplementary material available at https://doi.org/10.1186/s12917-023-03588-2.

Additional file 1: Figure S1. Validation of untargeted metabolomics using quality control (QC) samples. The correlation heat map showed the correlation coefficient among QC samples in both ionization modes.

Additional file 2: Figure S2. The permutation test of the orthogonal partial least squares discriminant analysis (OPLS-DA) model. The arrows show the results from the data compared with frequency histograms of the scores from 1000 permutations of the data which show the expected distribution of scores if no association exists. The x-axis represents the accuracy of the model. The y-axis represents the frequency of the model accuracy from 1000 permutations of the data.

Additional file 3: Figure S3. KEGG pathway for fructose and mannose metabolism. The differentially expressed metabolite (DEM), D-(-)-Mannitol, is highlighted in green.

Additional file 4: Figure S4. KEGG pathway for phosphotransferase system (PTS). The differentially expressed metabolite (DEM), D-(-)-Mannitol, is highlighted in green.

Additional file 5: Figure S5. KEGG pathway for β-alanine metabolism. The differentially expressed metabolite (DEM), spermine, is highlighted in red.

Additional file 6: Figure S6. KEGG pathway for arginine and proline metabolism. The differentially expressed metabolite (DEM), spermine, is highlighted in red.

Additional file 7: Figure S7. Quantification of key metabolites involved in arginine metabolism by targeted metabolomics. Differences between mean values were assessed by two-tailed Student's *t*-test. $*p < 0.05$; $**p < 0.01$; $***p < 0.001$.

Additional file 8: Figure S8. KEGG pathway for methane metabolism. The differentially expressed metabolite (DEM), S-hydroxymethylglutathione (S-HMG), is highlighted in red.

Additional file 9: Figure S9. KEGG pathway for phenylalanine metabolism. The differentially expressed metabolite (DEM), phenylacetylglycine, is highlighted in green.

Additional file 10: Figure S10. KEGG pathway for glycolysis/gluconeogenesis. The differentially expressed metabolite (DEM), 2,3-bisphospho-D-glyceric acid (2,3-BPG or glycerate-2,3P_2), is highlighted in red

Additional file 11: Table S1. Summary of the number of differentially expressed metabolites (DEMs) in each comparison group in both negative and positive ion modes

Additional file 12: Table S2. List of differentially expressed metabolites (DEMs) upon 6 h IFN-γ treatment compared to control in both negative and positive ion modes.

Additional file 13: Table S3. List of differentially expressed metabolites (DEMs) upon 12 h IFN-γ treatment compared to control in both negative and positive ion modes.

Additional file 14: Table S4. List of differentially expressed metabolites (DEMs) upon 24 h IFN-γ treatment compared to control in both negative and positive ion modes.

Additional file 15: Table S5. List of differentially expressed metabolites (DEMs) upon 12 h IFN-γ treatment compared to 6 h IFN-γ treatment in both negative and positive ion modes.

Additional file 16: Table S6. List of differentially expressed metabolites (DEMs) upon 24 h IFN-γ treatment compared to 6 h IFN-γ treatment in both negative and positive ion modes.

Additional file 17: Table S7. List of differentially expressed metabolites (DEMs) upon 24 h IFN-γ treatment compared to 12 h IFN-γ treatment in both negative and positive ion modes.

Acknowledgements
We thank Prof. Guoqiang Zhu (Yangzhou University, Yangzhou, China) for providing the MAC-T cell line. We also thank Kanehisa Laboratories for the permission of using the KEGG pictures in this study.

Authors' contributions
Conceptualization, L.L. and J.H; Methodology, F.L., X.H., Z.W., Q.Y., Q.S., W.R., T.W., Z.J. and N.L.; Software, F.L., X.H. and Q.Y.; Validation, F.L., X.H. and Z.W.; Formal Analysis, F.L., X.H., and L.L.; Investigation, F.L. and X.H.; Resources, J.H. and L.L.; Data Curation, F.L. and X.H.; Writing – Original Draft Preparation, F.L.; Writing – Review & Editing, F.L., J.H. and L.L.; Supervision, F.L., J.H. and L.L.; Project Administration, L.L.; Funding Acquisition, L.L. All authors contributed to the article and approved the final version of submitted manuscript.

Funding
This work was supported by the Natural Science Foundation of China (No. 31772715) and the Project of Jilin Provincial Department of Science and Technology (No. 20200404167YY).

Availability of data and materials
Different metabolites expression profiles identified by untargeted metabolomics in each comparison group has been deposited in Zenodo (https://doi.

org/10.5281/zenodo.5880761; https://doi.org/10.5281/zenodo.5880787) and summarized information has been uploaded to Figshare (https://doi.org/10.6084/m9.figshare.20898301.v1). All other data supporting the conclusions of this article is included within the article and its additional file.

Declarations

Ethics approval and consent to participate
Not applicable.

Consent for publication
Not applicable.

Competing interests
The authors declare no conflict of interest.

Received: 10 September 2022 Accepted: 24 January 2023
Published online: 11 February 2023

References

1. Patel JJ, Miller KR, Rosenthal C, Rosenthal MD. When Is It Appropriate to Use Arginine in Critical Illness? Nutr Clin Pract. 2016;31(4):438–44.
2. Morris SM Jr. Arginine: beyond protein. Am J Clin Nutr. 2006;83(2):508s–12s.
3. Morris SM Jr. Arginine metabolism: boundaries of our knowledge. J Nutr. 2007;137(6 Suppl 2):1602s–9s.
4. Albaugh VL, Pinzon-Guzman C, Barbul A. Arginine-Dual roles as an onconutrient and immunonutrient. J Surg Oncol. 2017;115(3):273–80.
5. Rodriguez PC, Ochoa AC, Al-Khami AA. Arginine Metabolism in Myeloid Cells Shapes Innate and Adaptive Immunity. Front Immunol. 2017;8:93.
6. Tabe Y, Lorenzi PL, Konopleva M. Amino acid metabolism in hematologic malignancies and the era of targeted therapy. Blood. 2019;134(13):1014–23.
7. Qiu F, Huang J, Sui M. Targeting arginine metabolism pathway to treat arginine-dependent cancers. Cancer Lett. 2015;364(1):1–7.
8. Qiu F, Chen YR, Liu X, Chu CY, Shen LJ, Xu J, Gaur S, Forman HJ, Zhang H, Zheng S et al: Arginine starvation impairs mitochondrial respiratory function in ASS1-deficient breast cancer cells. Science signaling 2014, 7(319):ra31.
9. Dillon BJ, Prieto VG, Curley SA, Ensor CM, Holtsberg FW, Bomalaski JS, Clark MA. Incidence and distribution of argininosuccinate synthetase deficiency in human cancers: a method for identifying cancers sensitive to arginine deprivation. Cancer. 2004;100(4):826–33.
10. Cao Y, Feng Y, Zhang Y, Zhu X, Jin F. L-Arginine supplementation inhibits the growth of breast cancer by enhancing innate and adaptive immune responses mediated by suppression of MDSCs in vivo. BMC Cancer. 2016;16:343.
11. Liu B, Che Y, Zhang M, Ren W, Xia X, Liu H, Huang T, Huang J, Lei L. IFN-γ Activates the TLR4-CCL5 Signaling Through Reducing Arginine Level, Leading to Enhanced Susceptibility of Bovine Mammary Epithelial Cells to Staphylococcus aureus. Inflammation. 2020;43(6):2209–21.
12. Schroder K, Hertzog PJ, Ravasi T, Hume DA. Interferon-gamma: an overview of signals, mechanisms and functions. J Leukoc Biol. 2004;75(2):163–89.
13. Kak G, Raza M, Tiwari BK. Interferon-gamma (IFN-γ): Exploring its implications in infectious diseases. Biomol Concepts. 2018;9(1):64–79.
14. Antvorskov JC, Fundova P, Buschard K, Funda DP. Dietary gluten alters the balance of pro-inflammatory and anti-inflammatory cytokines in T cells of BALB/c mice. Immunology. 2013;138(1):23–33.
15. Lamas B, Vergnaud-Gauduchon J, Goncalves-Mendes N, Perche O, Rossary A, Vasson MP, Farges MC. Altered functions of natural killer cells in response to L-Arginine availability. Cell Immunol. 2012;280(2):182–90.
16. Xia XJ, Gao YY, Zhang J, Wang L, Zhao S, Che YY, Ao CJ, Yang HJ, Wang JQ, Lei LC. Autophagy mediated by arginine depletion activation of the nutrient sensor GCN2 contributes to interferon-γ-induced malignant transformation of primary bovine mammary epithelial cells. Cell Death Discov. 2016;2:15065.
17. Xia X, Che Y, Gao Y, Zhao S, Ao C, Yang H, Liu J, Liu G, Han W, Wang Y, et al. Arginine Supplementation Recovered the IFN-γ-Mediated Decrease in Milk Protein and Fat Synthesis by Inhibiting the GCN2/eIF2α Pathway, Which Induces Autophagy in Primary Bovine Mammary Epithelial Cells. Mol Cells. 2016;39(5):410–7.
18. Rhee K. Minding the gaps: metabolomics mends functional genomics. EMBO Rep. 2013;14(11):949–50.
19. Hong J, Yang L, Zhang D, Shi J. Plant Metabolomics: An Indispensable System Biology Tool for Plant Science. Int J Mol Sci. 2016;17(6):767.
20. Zhao YY, Wu SP, Liu S, Zhang Y, Lin RC. Ultra-performance liquid chromatography-mass spectrometry as a sensitive and powerful technology in lipidomic applications. Chem Biol Interact. 2014;220:181–92.
21. Kanehisa M, Goto S. KEGG: kyoto encyclopedia of genes and genomes. Nucleic Acids Res. 2000;28(1):27–30.
22. Kanehisa M. Toward understanding the origin and evolution of cellular organisms. Protein science : a publication of the Protein Society. 2019;28(11):1947–51.
23. Kanehisa M, Furumichi M, Sato Y, Kawashima M, Ishiguro-Watanabe M. KEGG for taxonomy-based analysis of pathways and genomes. Nucleic Acids Res. 2023;51(D1):D587-d592.
24. Zou Y, Shao J, Li Y, Zhao FQ, Liu JX, Liu H. Protective Effects of Inorganic and Organic Selenium on Heat Stress in Bovine Mammary Epithelial Cells. Oxid Med Cell Longev. 2019;2019:1503478.
25. Li L, Li F, Hu X, Wu Z, Ren W, Wang T, Ji Z, Li N, Gu J, Sun C, et al. LAP3 contributes to IFN-γ-induced arginine depletion and malignant transformation of bovine mammary epithelial cells. BMC Cancer. 2022;22(1):864.
26. Chen M, Zhang W, Wu H, Guang C, Mu W. Mannitol: physiological functionalities, determination methods, biotechnological production, and applications. Appl Microbiol Biotechnol. 2020;104(16):6941–51.
27. Southern KW, Clancy JP, Ranganathan S. Aerosolized agents for airway clearance in cystic fibrosis. Pediatr Pulmonol. 2019;54(6):858–64.
28. Ren W, Li Y, Xia X, Guo W, Zhai T, Jin Y, Che Y, Gao H, Duan X, Ma H, et al. Arginine inhibits the malignant transformation induced by interferon-gamma through the NF-κB-GCN2/eIF2α signaling pathway in mammary epithelial cells in vitro and in vivo. Exp Cell Res. 2018;368(2):236–47.
29. Soda K. The mechanisms by which polyamines accelerate tumor spread. J Exper Clin Cancer Res. 2011;30(1):95.
30. Childs AC, Mehta DJ, Gerner EW. Polyamine-dependent gene expression. Cell Mol Life Sci. 2003;60(7):1394–406.
31. Gerner EW, Meyskens FL Jr. Polyamines and cancer: old molecules, new understanding. Nat Rev Cancer. 2004;4(10):781–92.
32. Miao J, Li F, Zhang M, Zhou C, Ren W, Hu X, Li N, Lei L. Carnosine Synthase 1 Contributes to Interferon Gamma-Induced Arginine Depletion via Mitogen-activated Protein Kinase 11 Signaling in Bovine Mammary Epithelial Cells. J Interferon Cytokine Res. 2022;42(9):501–12.
33. Barnett SD, Buxton ILO. The role of S-nitrosoglutathione reductase (GSNOR) in human disease and therapy. Crit Rev Biochem Mol Biol. 2017;52(3):340–54.
34. Beppu T, Nishi K, Imoto S, Araki W, Setoguchi I, Ueda A, Suetsugi N, Ishima Y, Ikeda T, Otagiri M et al: Novel nitric oxide donor, nitrated phenylbutyrate, induces cell death of human pancreatic cancer cells and suppresses tumor growth of cancer xenografts. Oncology reports 2022, 48(4):178.
35. Lu K, Ye W, Gold A, Ball LM, Swenberg JA. Formation of S-[1-(N2-deoxyguanosinyl)methyl]glutathione between glutathione and DNA induced by formaldehyde. J Am Chem Soc. 2009;131(10):3414–5.
36. Huang CK, Sun Y, Lv L, Ping Y. ENO1 and Cancer. Molecular therapy oncolytics. 2022;24:288–98.
37. Chen JM, Chiu SC, Chen KC, Huang YJ, Liao YA, Yu CR. Enolase 1 differentially contributes to cell transformation in lung cancer but not in esophageal cancer. Oncol Lett. 2020;19(4):3189–96.
38. Delaney J, Neville WA, Swain A, Miles A, Leonard MS, Waterfield CJ. Phenylacetylglycine, a putative biomarker of phospholipidosis: its origins and relevance to phospholipid accumulation using amiodarone treated rats as a model. Biomarkers. 2004;9(3):271–90.
39. Wang XS, Hu MX, Guan QX, Men LH, Liu ZY: Metabolomics analysis reveals the renal protective effect of Panax ginseng C. A. Mey in type 1 diabetic rats. Chin J Nat Med 2022, 20(5):378–386.
40. Leitão C, Matos B, Roque F, Herdeiro MT, Fardilha M: The Impact of Lifestyle on Prostate Cancer: A Road to the Discovery of New Biomarkers. J Clin Med 2022, 11(10):2925.

Publisher's Note